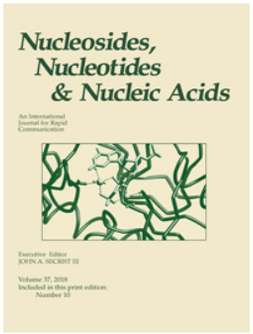

Nucleosides, Nucleotides and Nucleic Acids

ISSN: 1525-7770 (Print) 1532-2335 (Online) Journal homepage: https://www.tandfonline.com/loi/lncn20

DNA interaction studies of rhenium compounds with Schiff base chelates encompassing biologically relevant moieties

Muhammed Bilaal Ismail, Irvin Noel Booysen & Matthew Piers Akerman

To cite this article: Muhammed Bilaal Ismail, Irvin Noel Booysen & Matthew Piers Akerman (2019): DNA interaction studies of rhenium compounds with Schiff base chelates encompassing biologically relevant moieties, Nucleosides, Nucleotides and Nucleic Acids, DOI: 10.1080/15257770.2019.1639058

To link to this article: https://doi.org/10.1080/15257770.2019.1639058

Published online: 10 Jul 2019.

NUCLEOSIDES, NUCLEOTIDES AND NUCLEIC ACIDS
https://doi.org/10.1080/15257770.2019.1639058

DNA interaction studies of rhenium compounds with Schiff base chelates encompassing biologically relevant moieties

Muhammed Bilaal Ismail, Irvin Noel Booysen, and Matthew Piers Akerman

School of Chemistry and Physics, University of KwaZulu-Natal, Pietermaritzburg, South Africa

ABSTRACT

Herein, we report the DNA interaction studies of rhenium(I) and -(V) compounds with Schiff base chelates encompassing biologically relevant moieties. More specifically, the DNA interaction capabilities of these rhenium complexes were probed using Gel Electrophoresis and Calf Thymus–DNA titrations monitored by temperature-controlled electronic spectroscopy. The DNA binding modes of the metal compounds were corroborated by molecular docking simulations. In addition, the synthesis and characterization of a novel *facial* tricarbonyl rhenium(I) compound, *fac*-[Re(chrs)$(CO)_3$Br], (chrs = {3-{[(2-hydroxyphenyl)imino]methyl}-4*H*-chromen-4-one) are reported.

ARTICLE HISTORY
Received 17 January 2018
Accepted 29 June 2019

KEYWORDS
DNA interaction; gel electrophoresis; molecular docking; rhenium; Schiff base

Introduction

The interaction of transition metal complexes towards DNA is a central scientific focus due to its relevance in cancer research and molecular biology.[1,2] Metal ions and their complexes can interact with DNA covalently and/or non-covalently; therefore, an understanding on their binding modes is particularly important for the design of modern metallopharmaceuticals.[3] Covalent bonding of a metal complex to the DNA double helix is typically initiated by substitution of a labile co-ligand within the coordination sphere of the metal complex followed by coordination of the metal centre to a nitrogen donor of a DNA nucleotide base. Non-covalent intercalative interactions are found in the form of $\pi \rightarrow \pi^*$ stacking between the *pi*-conjugated chromophores of metal complexes and DNA nucleotide bases.[4] In addition, non-covalent groove-binding occurs *via* van der Waals and hydrogen- or hydrophobic-interactions along the major or minor groove of the DNA double helix. Lastly, electrostatic interactions can be induced by columbic forces between a metal complex and the negatively-charged phosphate backbone of DNA.[4–6]

CONTACT Irvin Noel Booysen Booyseni@ukzn.ac.za School of Chemistry and Physics, University of KwaZulu-Natal, *Private Bag* X01, Scottsville, Pietermaritzburg, 3209, South Africa.
Color versions of one or more of the figures in the article can be found online at www.tandfonline.com/lfnn.
Supplemental data for this article is available online at https://doi.org/10.1080/15257770.2019.1639058.

Rhenium exhibits diverse coordination chemistry and its organometallic complexes have been utilized in myriad medicinal applications.[7–10] In particular, the β-emitting 186- and 188-rhenium radionuclides have optimal half-lives and energies which are ideally suited for the development of therapeutic radiopharmaceuticals.[11] However, the pharmacological efficacies of rhenium radiopharmaceuticals are typically poor, which is largely attributed to their lack of target-specificity. To address this concern, radiolabelling of multidentate chelators encompassing various biologically active moieties can be conducted.[12–14] Subsequently, the bio-active groups of these next-generation rhenium radiopharmaceuticals could facilitate well-defined biodistribution patterns and facile interaction with mutated DNA (*i.e.* malignant growths) at the target sites.[14]

In comparison with other metals, DNA interaction studies of rhenium compounds have not been widely reported and to the best of our knowledge, these research findings represent one of few studies reported on the interactions between rhenium(V) complexes and calf-thymus (CT)–DNA. In addition, gel-electrophoresis studies were conducting using CT–DNA with the individual rhenium(I) and -(V) Schiff base compounds containing nucleotide bases, benz(imidazole/othiazole) or chromone moieties: *trans*-[Re(ddd)(Hduo)$(PPh_3)_2$]I (**1**) (H_2ddd = 5,6-diamino-1,3-dimethyl uracil and H_3duo = [*N*-(2-hydroxybenzylidene)-5-amino-1,3-dimethyl uracil]); *fac*-[Re$(CO)_3$Br(adp)] (**2**) (adp = {5-amino-1,3-dimethyl-6-[(*Z*)-(pyridin-2-ylmethylidene)amino]pyrimidine-2,4(1*H*,3*H*)-dione}); *fac*-[Re$(CO)_3$Br(aap)] (**3**) (aap = {4-[(*Z*)-(2-aminobenzylidene)amino]pyrimidin-2(1*H*)-one}); *cis*-[Re(bcp)$OCl_2(PPh_3)$] (**4**) (Hbcp = [*N*-(2-hydroxybenzylidene)-benzothiazole]) (μ-bzp)$_2$[Re$(CO)_3]_2$; (**5**) (Hbzp = [*N*-(2-hydroxybenzylidene)-benzimidazole]); *fac*-[Re$(CO)_3$(bzch)Cl] (**6**) (bzch = (2-benzimidazole-4*H*-chromen-4-one)); *fac*-[Re$(CO)_3$(bsch)Cl] (**7**) (bsch = 2-benzothiazole-4*H*-chromen-4-one); [ReO(Hns)] (**8**) (Hns = *bis*-[(2-phenylthiolate)iminomethyl]-methyl-1-(2-hydroxyphenyl)prop-2-en-1-one) and [ReO(OCH_3) (PPh_3)(Huch-OCH_3)] (**9**) (H_2uch = [5-(6-amino-1,3-dimethyluracil)iminomethyl-4*H*-chromen-4-one]).[15]

This research studies serves as an evolution of our recent reports, whereby the rhenium compounds listed above have been previously reported and now have their DNA interaction capabilities investigated by UV–Vis titrations, gel-electrophoresis and molecular docking studies. Furthermore, the *facial* tricarbonyl rhenium(I) compound, *fac*-[Re(chrs)$(CO)_3$Br] (**10**), (chrs = {3-{[(2-hydroxyphenyl)imino]methyl}-4*H*-chromen-4-one}, see Figure 1) has not been previously reported and hence in addition to its DNA interaction studies, its synthesis, characterization and crystal data are included. Moreover, this investigation provides a comprehensive understanding with respect to the DNA binding capabilities of

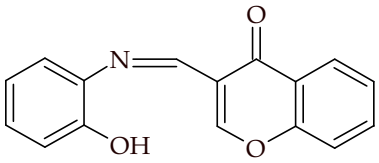

Figure 1. Structure of chrs.

the rhenium compounds **1–9** and provides impetus to explore their *in vitro* cytotoxicity and applied radiochemistry. Of particular significance is how the diverse coordination environments of the respective rhenium(I) and -(V) centres, as well as the varying stereo-electronic properties of the different bio-relevant chelators, dictated the DNA interaction modes of the corresponding metal complexes.

2. Experimental

2.1. Materials and methods

Ammonium perrhenate, rhenium pentacarbonyl bromide, rhenium pentacarbonyl chloride triphenylphosphine, hydrochloric acid, hydrobromic acid, hydroiodic acid, 3-formylchromone, 5,6-diamino-1,3-dimethyluracil, 2-aminobenz(othiazole/imidazole), cytosine, salicylaldehyde, 2-aminobenzaldehyde, picolinaldehyde, 1,2-diaminobenzene, 2-aminophenol, 2-aminothiophenol, trifluoroacetic acid, phosphate-buffered saline (PBS) tablets and calf thymus (CT)–DNA were obtained from Sigma Aldrich. The oxorhenium(V) precursors were synthesized as described by literature methods.[16] DNA chips, DNA 1 K gel and stain, DNA ladder and loading buffer were all obtained within a DNA 1 K Analysis Kit from Bio-Rad. All solvents were obtained from Merck SA. These chemicals were used without any further purification. The infrared spectra were recorded on a Perkin–Elmer Spectrum 100 from 4000 to 650 cm^{-1}. ^{1}H NMR spectra were obtained using a Bruker Avance 400 MHz spectrometer. All NMR spectra were recorded in DMSO-d6. UV–Vis spectra were recorded using a Perkin–Elmer Lambda 25. Melting points were determined using a Stuart SMP3 melting point apparatus. The conductivity measurements were determined at 295 K on a Radiometer R21M127 CDM 230 conductivity and pH meter. Toluene was dried with sodium wire and stored in the presence of dry 4 Å microsieves. The redox properties of the metal complexes were investigated by cyclic and square wave voltammetry. The concentration of the metal complexes was 2 mM and tetrabutylammoniumtetrafluoroborate (0.1 M) was used as the supporting electrolyte. A Metrohm Autolab Potentiometer was used for measurements equipped with a three-electrode

system: pseudo Ag|AgCl reference electrode, a glassy carbon working electrode and Pt auxiliary counter electrode.

2.2. Synthesis of 3-{[(2-hydroxyphenyl)imino]methyl}-4H-chromen-4-one (chrs)

Equimolar amounts of 2-aminophenol (157 mg; 1.44 mmol) and 3-formylchromone (250 mg; 1.44 mmol) were added to 20 cm^3 of methanol and heated until reflux for 3 hours. A large quantity of brown precipitate was filtered, washed with 3×2 cm^3 of cold methanol and 2×3 cm^3 of petroleum ether and left to dry in desiccator. Yield: 92%. M.P: 202.4–205.8 °C. IR (ν_{max}/cm^{-1}): ν(O–H) 3160 w, ν(C = O) 1639 s, ν(C = N) 1549 s. ^{1}H NMR (303 K ppm^{-1}): 10.29 (br s, 1 H, *OH*), 8.16 (d, 1 H, *H8*), 7.86 (d, 1 H, *H11*), 7.58–7.44 (m, 2 H, *H9*, *H10*), 7.09–7.18 (m, 2 H, *H4*, *H5*), 6.99–6.92 (m, 2 H, *H1*, *H2*), 6.87 (t, 1 H, *H3*), 5.84 (s, 1 H, *H6*). UV–Vis (MeOH, λ_{max} (ε, M^{-1} cm^{-1})): 243 nm (6505), 268 nm (5692), 312 nm (2434), 404 nm (17280).

2.3. Synthesis of fac-[Re(chrs)(CO)$_3$Br] (10)

The ligand chrs (65.3 mg, 246 µmol) was added to [Re(CO)$_5$Br] (100 mg, 246 µmol) in 20 cm^3 of dry toluene. The resultant mixture was heated at reflux temperature under an inert N_2 atmosphere for 4 hours. A dark green precipitate was filtered and dried overnight in a desiccator. This precipitate was dissolved in dichloromethane and layered with *n*-hexane from which yellow parallelogram-shaped crystals grew after five days. Yield: 72%. M.P: 286.4–289.2 °C. IR (ν_{max}/cm^{-1}): ν(O–H) 3318 w, ν(C≡O)$_{fac}$ 2020 and 1878 s, ν(C = O) 1632 m, ν(C = N) 1557 m. ^{1}H NMR (303 K ppm^{-1}): 9.95 (br s, 1 H, O*H*), 9.42 (s, 1 H, *H1*), 8.56 (s, 1 H, *H6*), 8.32 (d, 1 H, *H8*), 8.14 (t, 1 H, *H9*), 8.01 (d, 1 H, *H11*), 7.69 (t, 1 H, *H10*), 7.28 (d, 1 H, *H5*), 7.13 (t, 1 H, *H4*), 7.00 (d, 1 H, *H2*), 6.89 (t, 1 H, *H3*). UV–Vis (DMF, λ_{max} (ε, M^{-1} cm^{-1})): 242 nm (17248), 260 nm (14836), 284 nm (16824), 320 nm (12429), 395 (12042). Conductivity (DMF, 10^{-3} M) = 8.64 Ω^{-1} cm^{-2} mol^{-1}.

2.4. X-ray crystallography

The X-ray data for the metal complex **10** was recorded on a Bruker Apex Duo equipped with an Oxford Instruments Cryojet operating at 100 K and an Incoatec microsource operating at 30 W power. Crystal and structure refinement data are given in Table 1 and selected bond lengths and angles for **10** are given in Table 2. The data were collected with Mo Kα ($\lambda = 0.71073$ Å) radiation at a crystal-to-detector distance of 50 mm.

Table 1. Crystal data and structure refinement data for compound **10**.

Chemical formula	$C_{19}H_{11}NO_6ReBr$
Formula weight	615.40
Temperature (K)	100
Crystal system	Monoclinic
Space group	$P2_1/n$
Unit cell dimensions (Å, °)	$a = 7.4735(4)$
	$b = 14.4084(7)$
	$c = 16.4626(7)$
	$\beta = 96.997(3)$
V (Å^3)	1759.51(15)
Z	4
Density (calc.) (Mg m^{-3})	2.32
Absorption coefficient (mm^{-1})	9.22
$F(000)$	1160
θ range for data collection (°)	1.9-26.4
Index ranges	−8/6; -18/17; -20/20
Reflections measured	14593
Observed data [$I > 2\sigma(I)$]	2947
Data/restraints/parameters	3339/0/256
Goodness of fit on F^2	1.050
R, wR^2	0.0200, 0.042

Table 2. Selected bond lengths [Å] and bond angles [°] for **10**.

Re–C18	1.912(4)	C20–Re–O2	173.5(1)
Re–C19	1.908(3)	C19–Re–Br	174.2(1)
Re–C20	1.915(4)	O2–Re–N	84.2(1)
Re–Br	2.6327(5)	C13–O6	1.361(5)
Re–O2	2.136(2)	C19–O4	1.151(5)
Re–N	2.186(3)	C8–O2	1.257(4)
C18–Re–N	178.4(1)		

The following conditions were used for the Bruker data collection: omega and phi scans with exposures taken at 30 W X-ray power and 0.50° frame widths using APEX2.[17]. The data were reduced with the program SAINT[17] using outlier rejection, scan speed scaling, as well as standard Lorentz and polarization correction factors. A SADABS[17] semi-empirical multi-scan absorption correction was applied to the data.[18] Direct methods, SHELXS-97[19] and WinGX[20] were used to solve the structure. All non-hydrogen atoms were located in the difference density map and refined anisotropically with SHELXL-97.[19] All hydrogen atoms were included as idealized contributors in the least squares process. Their positions were calculated using a standard riding model with C–$H_{aromatic}$ distances of 0.93 Å and $U_{iso} = 1.2$ Ueq.

2.5. UV–Vis DNA binding titrations

CT–DNA was prepared in PBS at a pH of 7.2 and the DNA binding studies of the metal complexes were carried out in MeOH. The DNA solution afforded a ratio of UV absorbance at 260 and 280 nm of approximately 1.9:1 which indicates that the DNA was sufficiently free of protein.[21]

In addition, the CT–DNA concentration per nucleotide was determined by UV absorption spectroscopy using the molar absorption coefficient (ε_{260}=6600 M^{-1} cm^{-1}).[21] The resultant stock DNA solution was stored at a temperature of 4 °C and used within 2 days after preparation. Furthermore, the respective metal complexes and CT–DNA solutions were incubated for 24 hours at 25 °C prior to any UV–Vis measurements.[22] The UV–Vis spectra were attained for a solution of metal complex (of known concentration in methanol) with varying nucleotide concentrations (0–200 μM) in PBS. The data attained from the absorption titration experiments were fitted to the following equation to obtain the intrinsic binding constant (K_b):

$$\frac{[DNA]}{(\varepsilon_a - \varepsilon_f)} = \frac{[DNA]}{(\varepsilon_b - \varepsilon_f)} + \frac{1}{K_b(\varepsilon_b - \varepsilon_f)}.$$

In this equation, [DNA] is the concentration of DNA in base pairs, ε_a is the extinction coefficient of the observed absorption band at the given DNA concentration (corresponds to A_{obs}/[complex]), ε_f is the extinction coefficient of the complex free in solution, and ε_b is the extinction coefficient of the complex when fully bound to DNA. A plot of [DNA]/[ε_a – ε_f] versus [DNA] gave a slope 1/[ε_a – ε_f] and Y intercept equal to 1/K_b[ε_b – ε_f]. The intrinsic binding constant (K_b) is estimated to be the ratio of the slope to the intercept.[22]

2.6. Gel electrophoresis

A Bio-Rad Experion™ Automated Electrophoresis System was used to perform the CT gel electrophoresis study using the reagents and supplies from a Bio-Rad DNA 1 K kit. The system consists of the Experion™ electrophoresis, priming and vortex station. CT–DNA (2 mM, prepared in the same manner as for the DNA binding titrations) and the metal complexes (at different concentrations) were incubated at room temperature, 24 hours prior to analysis.

2.7. Computational studies

Computational calculations were conducted with GAUSSIAN 09W.[23] Geometry optimizations of the metal complexes were achieved through DFT calculations using the B3LYP functional, with an accompanying hybrid basis set *viz.* the 6-311G^{++} (*d, p*) basis set was applied to all the nonmetal atoms and the LANL2DZ basis set, which makes use of effective core potentials, applied to the metal centre.[24,25] The use of these computational settings was validated by the reasonable agreement between the

optimized and geometrical parameters. The minor deviations are attributed to the fact that gas phase optimized structures do not account for nonclassical hydrogen bonding interactions or any short distance contacts. Furthermore, the lack of any negative Eigen values in the frequency calculations confirmed that the optimized structures are at a global minima on the potential energy surfaces.[26] Molecular docking simulations were carried out using the optimized structures and the programme Patchdock Beta version 1.3. Molecular interactions were refined using Firedock[27] and visualizations were adapted through YASARA View.[28] The B–DNA structure (LOX) (PDB ID: 1F8N) was obtained from the Protein Data Bank and all water molecules were removed prior to the docking procedure.

3. Results and discussion

3.1. Synthesis and characterization of fac-[Re(chrs)(CO)$_3$Br] (10)

The equimolar coordination reaction between chrs and [Re(CO)$_5$Br] afforded an octahedral rhenium(I) complex, *fac*-[Re$^{\mathbf{I}}$(CO)$_3$Br(chrs)]. In contrast to the intra-ligand cyclization observed for the Hbcp and Hbzp chromone Schiff bases in the formation of **5** and **6**, the chrs chelator of **10** remained intact and coordinated as a neutral bidentate chelator *via* its $N_{imino}O_{ketonic}$ donor set. The compound is soluble in an array polar solvents such as alcohols, water, chlorinated and high-boiling point aprotic solvents. In addition, a low-molar conductivity value is observed due to this metal complex's charge neutrality.

The proton NMR spectrum of **10** shows well-resolved signals, which emphasizes the diamagnetic nature of the d^6 metal centre and are comparable to analogous signals found in the proton NMR spectrum of its free-ligand. In particular, broad O*H* singlets found at 8.16 and 9.95 ppm for ligand chrs and **10** (Figure S1) respectively, confirm that no cyclization of chrs took place upon coordination. Similarly, the shift of Schiff base singlet (found within a multiplet for chrs at 6.92–6.99 ppm) in comparison to **10** (9.42 ppm) is indicative of rhenium(I) coordination through the N_{imino} atom which further infers that no cyclization took place. The IR spectra for **10** are dominated by intense bands of the *facial* tricarbonyl co-ligands between 2020 and 1878 cm^{-1}. All the other bands associated with the chromone and heterocyclic moieties of **10** are found at medium intensity between 1639 and 1557 cm^{-1} (Figure S2).

In the UV–Vis spectrum, three absorbance maxima observed between 0 and 350 nm for **10** are ascribed to intraligand π–π^* transitions whereas the electronic transition at 395 nm is ascribed to a ligand-to-metal charge transfer band. For **10**, (Figure S3) the diffusion controlled processes at E_{pa}=0.02 and E_{pc}=–0.87 V are best described as a ligand induced oxidation

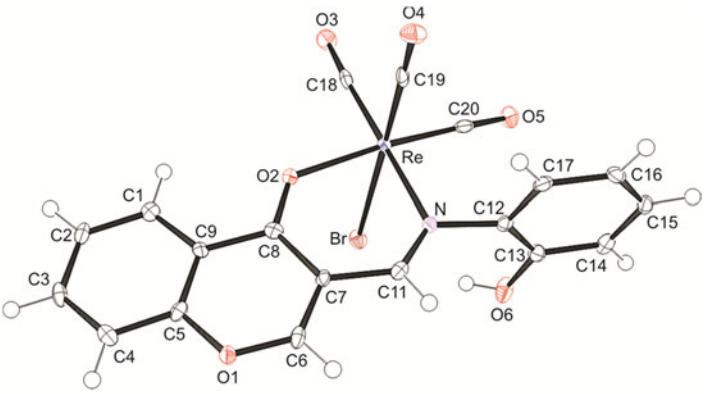

Figure 2. An ORTEP view of compound **10** showing 50% probability displacement ellipsoids and the atom labeling.

and reduction respectively, see Figure S4. The redox process at –1.12 V is tentatively attributed to a Re(I/0) reduction which falls within range for that of other tricarbonyl rhenium(I) compounds (–0.98 to –1.26 V versus Ag|AgCl) and an irreversible Re(I/II) oxidation process is observed at 0.80 V.[29]

3.2. Crystal structure of fac-[Re(CO)$_3$(chrs)Br] (10)

Compound **10** crystallizes out as a monomeric, neutral compound, see Figure 2. Four molecules of **10** occupy an asymmetric unit cell with a $P2_1/n$ space group. The Re–CO [1.906(3)–1.915(4) Å] and Re–Br [2.6327(5) Å] bonds within the coordination sphere are typical of *facial* tricarbonylrhenium(I) compounds, *e.g.* *fac*-[Re(CO)$_3$Br[(2-pyridylmethyl)NH$_2$]], *fac*-[Re(CO)$_3$[(2-pyridylmethyl)$_2$NH]]Br and their derivatives [Re–CO: 1.904(6)–1.927(4) Å, Re–Br: 2.618(1)–2.6462(7) Å].[30] The Re–O$_{ketonic}$ bond length of 2.136(2) Å compares well with that of **7** [2.147(2) Å][15] while the Re–N$_{imino}$ [2.186(3) Å] bond distance is within range found for other rhenium(I) Schiff base compounds [2.144(4)–2.194(5) Å].[31] Furthermore, the constrained O2–Re–N bite angle [84.2(1)°] induces non-linearity of the equatorial [C18–Re–N: 178.4(1)° and C20–Re–O2: 173.5(1)°] and axial [C19–Re–Br: 174.2(1)°] bond angles.

The deviation of the latter is further influenced by classical intramolecular hydrogen bonding [O6–H···Br = 2.5508(4) Å]. In addition, this hydrogen-bonding allows the chromone and phenol planes to lie almost perfectly perpendicular to each other (88.47°). Hybridization of the C–O bonds are clearly depicted when comparing the C13–O6 single bond length [1.361(5) Å] to the double bond C8–O2 [1.257(4) Å] and the carbonyl triple bond C19–O4 [1.151(5) Å]. In addition, the molecules pack along the

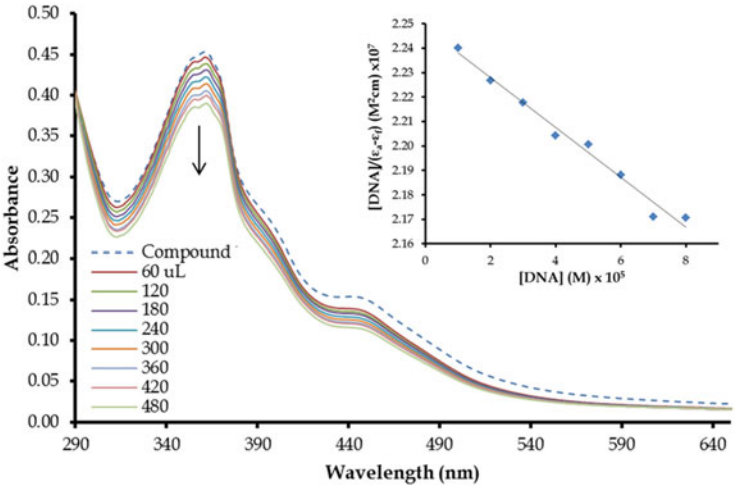

Figure 3. The overlay UV–Vis absorption spectra of compound **1.** The dashed line indicates complex **1** free of any DNA and the hypochromic effect (indicated by the arrow) is due to progressive increments of a 2 mM CT–DNA solution.

[*b*]-axis due to short contacts between adjacent phenol moieties [3.156(5)–3.382(4) Å] and adjacent C_{imine}···O3 atoms [3.079(4) Å] of neighbouring molecules.

3.3. DNA interaction studies of pyrimidine Schiff base rhenium compounds 1–3

Gradual electronic spectral changes upon the addition of increasing amounts of DNA is one of the most common methods used to determine the binding mode and extent of the interaction between inorganic or organic compounds with DNA. Upon the addition of CT–DNA, the absorption intensity of a metal complex may increase (hyperchromism), decrease (hypochromism) or cause a red-shift in absorption wavelength of a selected peak maximum (bathochromism). In general, hypochromism accompanied with bathochromism is associated with an intercalative binding mode of metal complexes in the DNA helix and involves a strong $\pi \rightarrow \pi^*$ stacking interaction between aromatic chromophores and the base pairs of DNA.[32,33] The DNA titration spectra for **1**, **2** and **3** are similar in that they each display hypochromism (between 15 and 20%) with zero or negligible bathochromic effects (**1**: 0%, **2**: 0%, **3**: 0.3%), see Figures 3, 4 and S5. The data were consistent for compounds of a DNA groove-binding nature *e.g.* the groove-binding metal complex, *fac*-[$Re(CO)_3$(phendione)Cl] {phendione = 1,10-phenanthroline-5,6-dione} which exhibits hypochromism (albeit 30%) and a negligible shift in absorption maximum wavelength.[22] In addition, the binding constants (K_b values) were calculated using the linear plot insets of [DNA]/[$\varepsilon_a - \varepsilon_f$] versus [DNA]. K_b was found

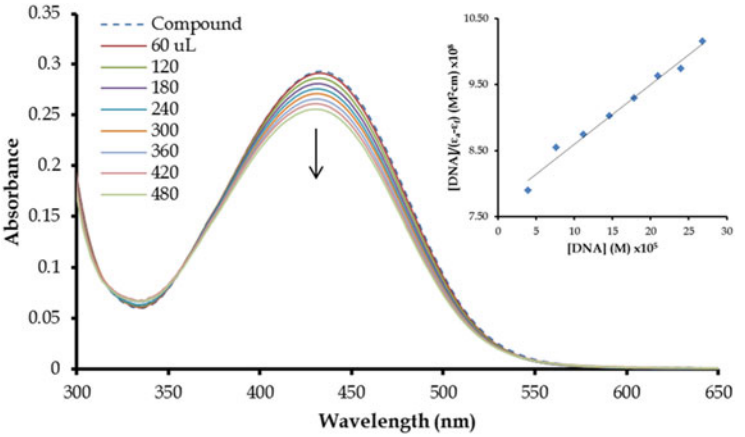

Figure 4. The overlay UV–Vis absorption spectra of compound **2.** The dashed line indicates complex **2** free of any DNA and the hypochromic effect (indicated by the arrow) is due to progressive increments of a 2 mM CT–DNA solution.

to be 1.01 (± 0.42)×0^3 M^{-1}, 1.17 (± 0.32)×10^3 M^{-1} and 2.75 (± 0.78)×10^5 M^{-1} for **1**, **2** and **3**, respectively. This compares well with literature metal complexes containing multidentate Schiff base ligands (10^3 M^{-1}>K_b>10^6 M^{-1}).[34–37]

Molecular docking is a well-established computational technique for predicting the best interaction between a metal complex and DNA to form a new DNA–metal complex conjugate of lowest possible energy.[38] Relatively smaller molecules tend to interact with the DNA minor groove due to minute steric interferences and generally the lowest energy metal complex–DNA adducts arises from metal complexes with freely rotational aromatic rings. Furthermore, these metal complexes can orientate to the curvature of the groove while displacing water molecules.[39] Molecular docking simulations conducted on **1**–**3** corroborated their experimental CT–DNA binding modes where computationally, all three metal complexes exhibit groove binding: **1** docks within the major groove of B–DNA (nucleotide base pairs: AT, AT, TA, TA, CG) and the other two metal compounds dock within the minor groove (nucleotide base pairs: GC, CG, GC). These metal compounds have lowest calculated global energies of –39.48, –47.65 and –40.03 kJ mol^{-1}, respectively (Figures 5, S6 and S7). The adducts of **2** and **3** with B–DNA are largely stabilized by hydrogen bonding: between the bromide co-ligand and guanine amine for **2** and the *axial* tricarbonyl co-ligand and a phosphate oxygen atom for **3**. This affords similarity between the configurations of the rhenium(I) compounds **2** and **3**, where both Schiff base chelators interact with the hydrophobic B–DNA interior and their more polar tricarbonyl moieties with the hydrophilic phosphate backbone.

As expected, compound **1** has a larger calculated van der Waals radius (8.798 Å) from its geometric centre in comparison to **2** and **3** (radii of

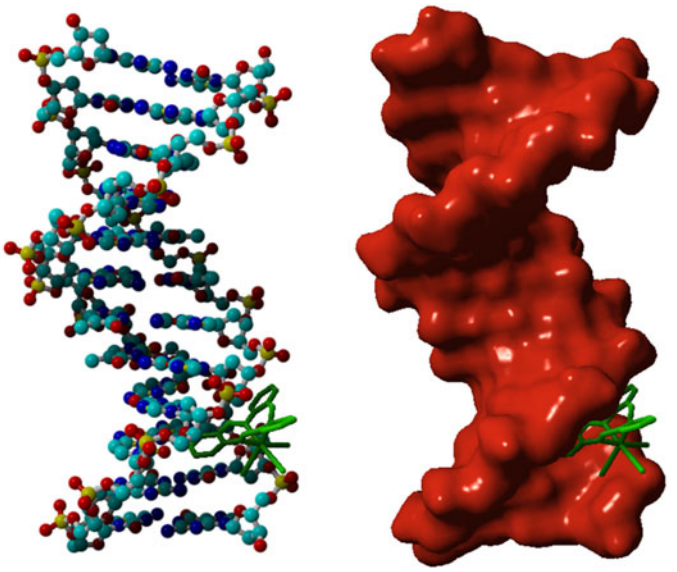

Figure 5. Docked position of **3** bound to the minor groove of B–DNA: ball and stick view (left) and DNA molecular surface view (right).

equal size, 7.037 Å) with steric hindrance of the bulky PPh_3 group rationalizing its affinity for the major groove of B–DNA instead of the minor groove. However, literature trends reveals that metal complexes with triphenylphosphines within their coordination spheres can bind within either the major or minor grooves of B–DNA, like in the case of the series of silver(I) complexes: $[AgCl(PPh_3)_2(MTZD)]$, $\{[AgCl(PPh_3)_2(MBZT)]$ and $[AgCl(PPh_3)_2(CMBZT)]$ (where MTZD = 2-mercaptothiazolidine, MBZT = 2-mercaptobenzothiazole and CMBZT = 5-chloro-2-mercaptobenzothiazole).[40] Further observation of the complex–DNA adduct of **1** reveals three firm intermolecular hydrogen bonds, arising from the uracil moiety of Hduo, stabilizes the DNA adduct of **1** and B–DNA in the major groove including the methyl carbons with thymine O_{ketone} atom (2.356 Å) and guanine ring nitrogen (2.207 Å) as well as O_{ketone} with adenine N_{amine} (2.012 Å).

Interestingly, even though the docked structures of **1** and **2** exhibit only a slightly lower energy than **3**, metal complexes **1** and **2** display a substantially lower experimental intrinsic binding constant (K_b) value. This would suggest that there is a combination of experimental factors for **1** and **2** to overcome to be able to dock in energetically favourable positions. Evaluating the structure of the Schiff base chelators for **1** and **2**, the uracil moieties each contain two polar ketone and two non-polar methyl groups. Thus, in order for the chelating moieties to facilitate groove-binding, the competitive polarity interactions must breach analogous interactions found within the interior and exterior of the CT–DNA double helix.

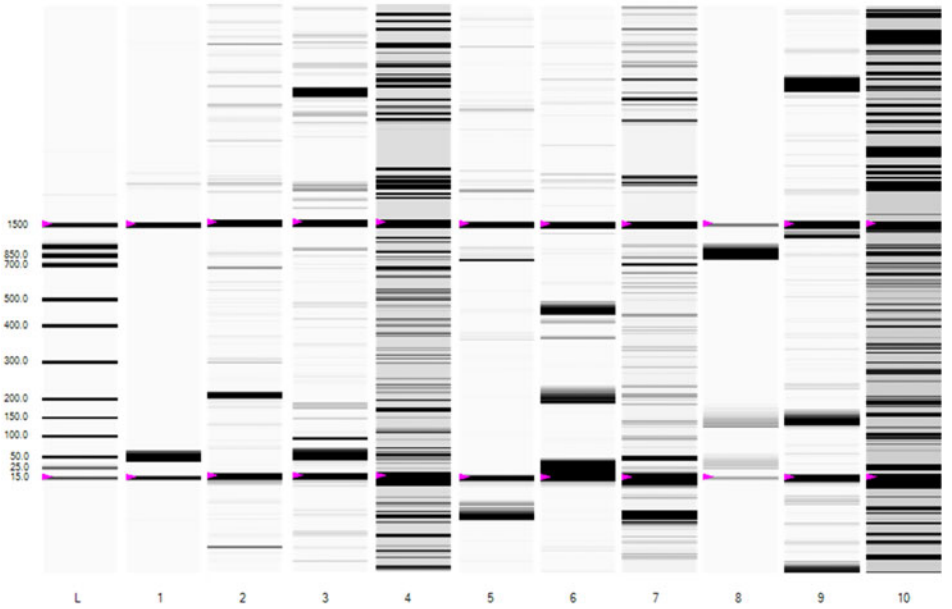

Figure 6. Lane L: DNA Ladder of known base pair lengths, Lane 1: CT DNA only, Lane 2: DNA + 10 μM of **1**, Lane 3: DNA + 50 μM of **1**, Lane 4: DNA + 100 μM of **1**; Lane 5: DNA + 10 μM of **2**, Lane 6: DNA + 50 μM of **2**, Lane 7: DNA + 100 μM of **2**; Lane 8: DNA + 10 μM of **3**, Lane 9: DNA + 50 μM of **3** and Lane 10: DNA + 100 μM of **3**.

A gel electrophoresis study was conducted to evaluate whether the groove-binding metal complexes induce DNA cleavage, see Figure 6. In comparison with CT–DNA only (Lane 1), it is seen that the cleaving ability of all three metal compounds correlate with increasing compound concentration. At the highest concentrations (Lanes 4, 7 and 10) compounds **1** and **3** display a similar activity, greater than that of **2**. This suggests that **1** and **3** are able to produce more DNA damaging reactive oxygen species than that of **2**. DNA fragments greater than 1500 bp are observed for **1**–**3** as CT–DNA contains DNA chains far greater in length than the limit of detection in this study.[41]

3.4. DNA interaction studies of benz(imidazole/othiazole) rhenium compounds 4–6

The overlay electronic spectra of **4**–**6** indicate no significant structural contusions as implied by the lack of red or blue shifts of peak maxima upon DNA addition (**4**: 0 nm, **5**: 3 nm bathochromism, **6**: 0 nm), see Figures S8–S10. However, compound **4** displays a substantial hyperchromic shift (∼20%) of the peak at 262 nm which is evidence for the formation of an adduct between this compound and the double-helical DNA.[42] This type of shift is further consistent for a metal complex of groove-binding nature,

as illustrated by cobalt(II) and nickel(II) complexes of salicylaldehyde 2-phenylquinoline-4-carboylhydrazone (H_2L) {$[M(HL)(H_2O)_3](NO_3)_2$ where M = Co or Ni}.[43] Compounds **5** and **6** are similar in that they display hypochromic effects, perhaps as a result from the contraction of DNA phosphate chains.[44,45]. Although **5** exhibits both properties of an intercalative complex, the minor observed red-shift coupled with the large dinuclear structure of **5** make this mode of interaction unlikely. Thus compounds **4–6** are designated as groove-binding compounds and exhibit binding constants {**4**: K_b=2.76 (± 0.94)×10^5 M^{-1}, **5**: K_b=4.32 (± 0.62)×10^3 M^{-1} and **6**: K_b=9.37 (± 0.55)×10^4 M^{-1}} which are comparable with other such metal compounds found in literature (K_b: 5.60 × 10^3–8.72 × 10^7 M^{-1}).[46,47]

Molecular docking studies of **4–6** show that all three metal compounds bind to the minor groove of B–DNA in the GC, CG, GC, CG region (Figures S11–S13). Compound **5** displays the highest global energy of the three compounds (**4**: –35.06, **5**: –28.14 and **6**: –47.38 kJ mol^{-1}) primarily due to its large dinuclear structure (van der Waals radius = 8.078 Å). Flexibility of molecules plays an important role in increasing molecule–DNA stability as they can orient more easily along the minor groove.[48,49] The rigidity of **5** may prevent manoeuvrability within the B–DNA minor groove and could further attest for its lower intrinsic binding constant. Compound **6** displays two strong bonding interactions: between its chlorine co-ligand and an outer $O_{phosphate}$ atom (2.300 Å) as well as a chromone carbon and guanine N_{amine} atom (2.533 Å). This bonding pattern results in **6** having the lowest energy of the three compounds. Compound **5** also exhibits two close contacts: a triphenylphosphine carbon atom with a guanosine ribose carbon atom (2.694 Å) and chlorine co-ligand with a ribose methyl moiety (2.616 Å). Despite the difference in global energies, compounds **4** and **6** display a similar calculated binding constant which suggests that there are dynamic factors for **6** to overcome to be able to dock in its energetically favourable position.[50]

It is common for transition metals to cleave DNA *via* metal-mediated radical production.[51] Compounds **4–6** were incubated with CT–DNA to preliminary assess if the groove-binding compounds are able to cleave DNA in this manner, which can further provide insight about their potential cytotoxicities.[52] From the virtual gel stain (Figure 7), it is seen that all three compounds exhibit substantial DNA cleavage. Compound **5** displays consistent cleaving ability at all three concentrations whereas compounds **4** and **6** show a positive cleaving correlation with concentration. Based on the number of dark bands (*i.e.* high DNA concentration) in the 0–50 bp region, compound **4** at 100 µM (lane 4) displays the most significant DNA cleaving ability which insinuates that

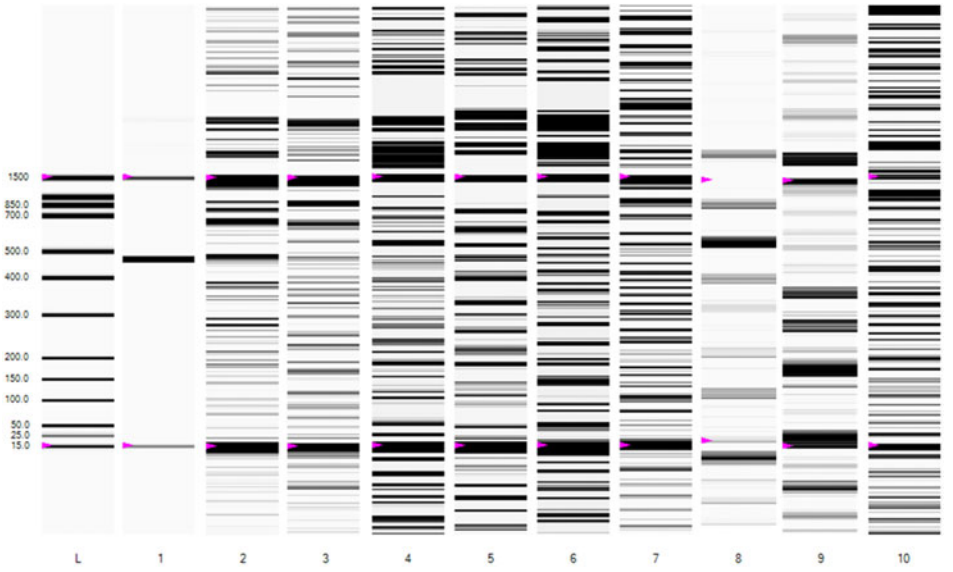

Figure 7. Lane L: DNA Ladder of known base pair lengths, Lane 1: CT DNA only, Lane 2: DNA + 10 μM of **4**, Lane 3: DNA + 50 μM of **4**, Lane 4: DNA + 100 μM of **4**; Lane 5: DNA + 10 μM of **5**, Lane 6: DNA + 50 μM of **5**, Lane 7: DNA + 100 μM of **5**; Lane 8: DNA + 10 μM of **6**, Lane 9: DNA + 50 μM of **6** and Lane 10: DNA + 100 μM of **6**.

it is able to generate more reactive oxygen species at high concentrations than **5** and **6**.[22,51]

3.5. DNA interaction studies of chromone Schiff base rhenium compounds 7–10

Compounds **7–10** induce no significant structural damage of the DNA–helix as indicated by a lack of substantial red or blue shifts of the peak maxima (see Figures S14–S17). Compounds **7–9** display hypochromism (**7**: 8%, **8**: 8% and **9**: 42%) whereas compound **10** exhibits hyperchromism (13%) as well as two isosbestic points at 303 and 349 nm. Isosbetic points are commonly seen in DNA binding titrations but do not infer binding mode. Typical examples of this phenomenon are observed for the titrations of octahedral Schiff base iron(II) compounds $[Fe(bsal)_2]\cdot 2H_2O$ and $[Fe(bsas)_2]\cdot H_2O$ {bsal = 2-[(*E*)-(5-bromo-2-hydroxybenzylidene)amino]propanoic acid and bsas = 2-[(*E*)-(5-bromo-2-hydroxybenzylidene)amino]butanedioic acid} with CT–DNA.[53] Since, **7–10** do not display large hypochromism coupled with bathochromic shifts (indicative of intercalation), they are assigned as DNA groove-binding in nature. With reference to **10**, another molecule that exhibits hyperchromism and assigned as a groove binding compound is 3,5,6-trichloro-2-pyridinol.[54] Furthermore, the calculated K_b values of 4.22 (± 0.38)×10^4 M^{-1}, 2.21 (± 0.46)×10^5 M^{-1},

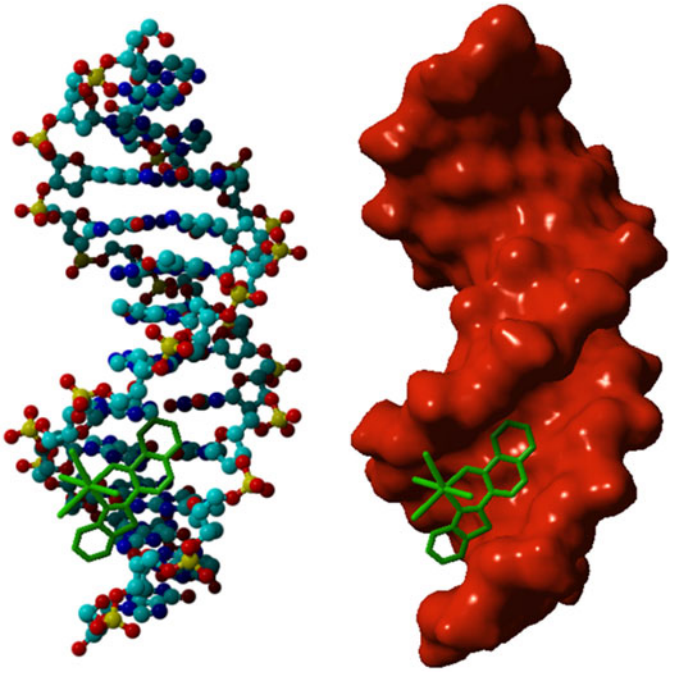

Figure 8. Docked position of **7** bound to the minor groove of B–DNA: ball and stick view (left) and DNA molecular surface view (right).

2.04 (±0.51)×10^5 M^{-1} and 1.96 (±0.25)×10^3 M^{-1}, for **7–10**, respectively, are well within the range of magnitudes previously described (Figure S18).

The relatively small rhenium(I) and -(V) complexes **7–10** [vdW radius *wrt.* geometric centre = 7.838 Å (for **7**), 8.123 Å (for **8**), 8.959 Å (for **9**) and 7.994 Å (for **10**)] makes this class of compounds groove-binding favourable (Figures 8, 9, S19 and S20). Compounds **7**, **8** and **10** interact with the minor groove of B–DNA within the AT, AT, GC, CG, GC, CG region whereas **9** docks within the major groove of the same region. All four compounds display high affinities for DNA based on their global lowest energies (**7**: –56.21, **8**: –59.72, **9**: –45.84, **10**: –47.47 kJ mol^{-1}) which supports the moderate to high K_b values attained during the experimental CT–DNA binding titrations. The structurally similar rhenium(I) compounds **7** and **10** indicate that the chromone moieties interact with the inner hydrophobic region of B–DNA and the metal carbonyls form hydrogen bonds with the hydrophilic phosphate backbone between 2.444 and 2.467 Å. In addition, compound **9** shows the higher energy than the other three compounds owing to its larger size and weaker interactions: it is stabilized by just a single hydrogen bond between a uracil O_{ketone} atom and phosphate oxygen atom (2.106 Å) whereas **7**, **8** and **10** each display at least two stabilizing hydrogen bonds (2.168–2.467 Å). Furthermore, compound **8** displays a unique square pyramidal geometry whereby the *axial* mono

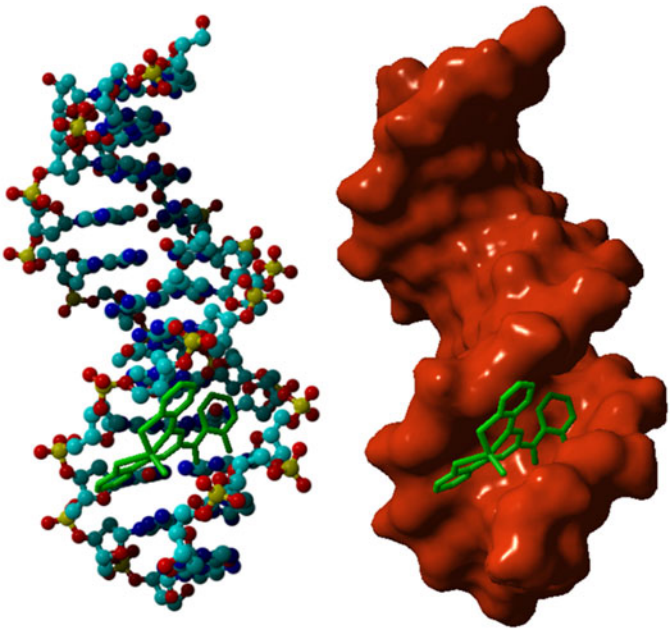

Figure 9. Docked position of **8** bound to the minor groove of B–DNA: ball and stick view (left) and DNA molecular surface view (right).

oxorhenium(V) core orientates away from the hydrophobic B–DNA interior with the tetradentate ligand moiety fitting along the carbon–phosphate backbone *via* numerous van der Waals interactions, resulting in the most energetically favourable complex–DNA adduct.

The virtual gel stains for compounds **7–10** clearly indicate that this class of metal complexes can substantially cleave CT–DNA (Figures 10 and 11). Upon observation of the lowest (0–100) bp regions of each compound, it is noted that compounds **8** and **10** cleave DNA to a similar extent across all three compound concentrations. In contrast, there is a visible increase in DNA cleavage activity upon increased concentration of **7** and **9**. The data suggest that the production of DNA-damaging reactive oxygen species are more concentration dependent for **7** and **9** and that at highest concentration (100 μM), all four compounds are able to cleave DNA to a similar extent.[42]

4. Conclusion

The molecular docking studies provided fascinating insight into the computational interactions between the metal compounds and B–DNA structure at the molecular level. Moreover, correlation could be found between the calculated global energies of the DNA–metal compound adducts and their experimental intrinsic binding constants. Of significance was the triphenylphosphine-containing rhenium(V) compounds **1**, **4** and **9** displaying the

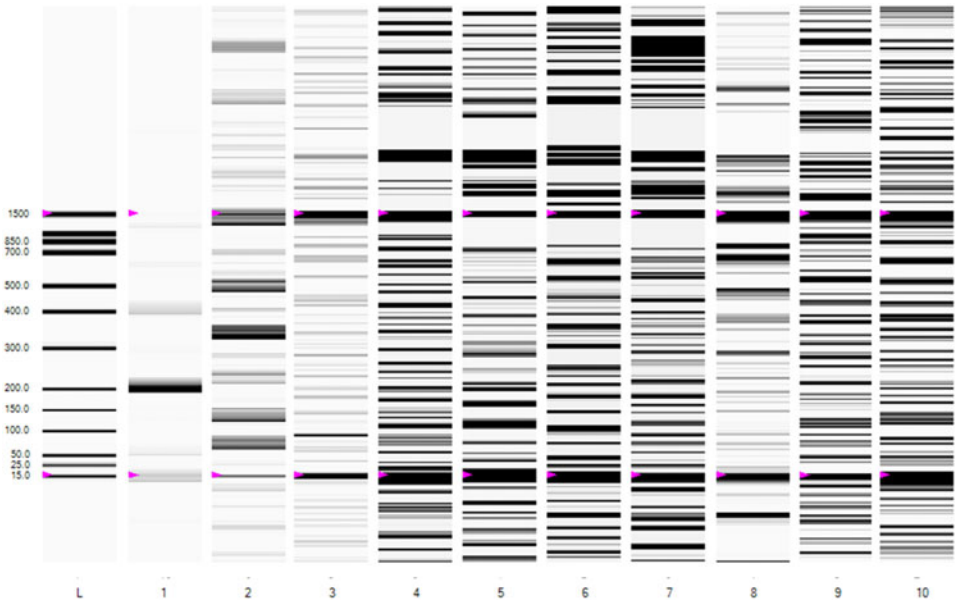

Figure 10. Lane L: DNA Ladder of known base pair lengths, Lane 1: CT DNA only, Lane 2: DNA + 10 μM of **7**, Lane 3: DNA + 50 μM of **7**, Lane 4: DNA + 100 μM of **7**; Lane 5: DNA + 10 μM of **8**, Lane 6: DNA + 50 μM of **8**, Lane 7: DNA + 100 μM of **8**; Lane 8: DNA + 10 μM of **9**, Lane 9: DNA + 50 μM of **9** and Lane 10: DNA + 100 μM of **9**.

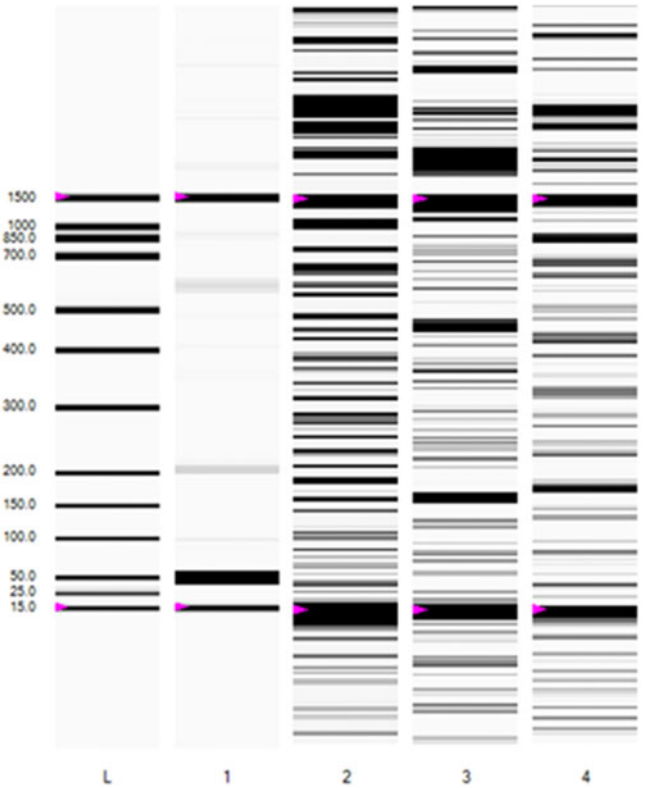

Figure 11. Lane L: DNA Ladder of known base pair lengths, Lane 1: CT DNA only, Lane 2: DNA + 10 μM of **10**, Lane 3: DNA + 50 μM of **10**, Lane 4: DNA + 100 μM of **10**.

ability to dock within either major or minor B–DNA grooves. It is also noted that the CT–DNA cleaving capability of the major groove binding compounds **1** and **9** do not significantly differ from the minor groove binding compound **4**. In addition, the square pyramidal geometry of the oxorhenium(V) complex **8** maximizes contact interaction between its tetradentate organic chelator and the B–DNA phosphate backbone, allowing an extension of the chelator to interact with the B–DNA interior. This research finding provides new scope for research in designing oxorhenium(V) complexes with similar chelating ligands whereby the resultant metal complexes could potentially circumvent the weak computational B–DNA interactions of these class of rhenium complexes as well as culminating low experimental intrinsic binding constants. Another interesting molecular docking research finding is with the competitive polarity interactions of the uracil derivatives (for **1** and **2**) to B–DNA which provides evidence for the low K_b values of **1** and **2**. Excluding compound **8**, the rhenium(I) compounds generally display superior affinities for DNA when compared to the rhenium(V) compounds stemming from their smaller vdW radii (*wrt* their geometries) and stronger bonding patterns between chelating ligands and the hydrophobic DNA interior.

Funding

We are grateful to the University of KwaZulu-Natal, the National Research Foundation of South Africa and the Deutscher Akademischer Austauschdienst (DAAD) for financial support.

References

[1] Hall, D.; Holmlin, R.; Barton, J. K. Oxidative DNA Damage Through Long-Range Electron Transfer. *Nature* **1996**, *382*, 731–735. DOI: 10.1038/382731a0.

[2] Yang, X.; Feng, J.; Zhang, J.; Zhang, Z.; Lin, H.; Zhou, L.; Yu, X. Synthesis, DNA Binding and Cleavage Activities of the Copper(II) Complexes of Estrogen-Macrocyclic Polyamine Conjugates. *Bioorg. Med. Chem.* **2008**, *16*, 3871–3877. DOI: 10.1016/j.bmc.2008.01.037.

[3] Clarke, M. J.; Sadler, P. J. *Metallopharmaceuticals I: DNA Interactions*; Springer: New York, **1999**.

[4] Pages, B. J.; Ang, D. L.; Wright, E. P.; Aldrich-Wright, J. R. Metal Complex Interactions with DNA. *Dalton Trans.* **2015**, *44*, 3505–3526. DOI: 10.1039/C4DT02700K.

[5] Zeglis, B. M.; Pierre, V. C.; Barton, J. K. Metallo-Intercalators and Metallo-Insertors. *Chem. Commun.* **2007**, *28*, 4565–4579. DOI: 10.1039/b710949k.

[6] Zhang, Q.; Liu, J.; Chao, H.; Xue, G.; Ji, L. DNA-Binding and Photocleavage Studies of Cobalt(III) Polypyridyl Complexes: $[Co(Phen)_2IP]^{3+}$ and $[Co(Phen)_2PIP]^{3+}$. *J. Inorg. Biochem.* **2001**, *83*, 49–55. DOI: 10.1016/S0162-0134(00)00132-X.

[7] Lee, L. C.-C.; Leung, K.-K.; Lo, K. K.-W. Recent Development of Luminescent Rhenium(I) Tricarbonyl Polypyridine Complexes as Cellular Imaging Reagents, Anticancer Drugs, and Antibacterial Agents. *Dalton Trans.* **2017**, *46*, 16357–16380. DOI: 10.1039/C7DT03465B.

[8] Gabr, M. T.; Pigge, F. C. Rhenium Complexes of Bis(Benzothiazole)-Based Tetraarylethylenes as Selective Luminescent Probes for Amyloid Fibrils. *Chem. Eur. J.* **2018**, *24*, 11729–11737. DOI: 10.1002/chem.201801801.

[9] Giffard, D.; Fischer-Fodor, E.; Vlad, C.; Achimas-Cadariu, P.; Smith, G. S. Synthesis and Antitumour Evaluation of Mono- and Multinuclear [2 + 1] Tricarbonylrhenium(I) Complexes. *Eur. J. Med. Chem.* **2018**, *157*, 773–781. DOI: 10.1016/j.ejmech.2018.08.011.

[10] Haase, A. A.; Bauer, E. B.; Kühn, F. E.; Crans, D. C. Speciation and Toxicity of Rhenium Salts, Organometallics and Coordination Complexes. *Coord. Chem. Rev.* **2019**, 394, 135–161. DOI: 10.1016/j.ccr.2019.05.012.

[11] Bauer, E. B.; Haase, A. A.; Reich, R. M.; Crans, D. C.; Kühn, F. E. Organometallic and Coordination Rhenium Compounds and Their Potential in Cancer Therapy. *Coord. Chem. Rev.* **2019**, *393*, 79–117. DOI: 10.1016/j.ccr.2019.04.014.

[12] Jürgens, S.; Herrmann, W. A.; Kühn, F. E. Rhenium and Technetium Based Radiopharmaceuticals: Development and Recent Advances. *J. Organomet. Chem.* **2014**, *751*, 83–89. DOI: 10.1016/j.jorganchem.2013.07.042.

[13] Abram, U.; Alberto, R. Technetium and Rhenium-Coordination Chemistry and Nuclear Medical Applications. *J. Braz. Chem. Soc.* **2006**, *8*, 1486–1500. DOI: 10.1590/S0103-50532006000800004.

[14] Makris, G.; Kuchuk, M.; Gallazzi, F.; Jurisson, S. S.; Smith, C. J.; Hennkens, H. M. Somatostatin Receptor Targeting with Hydrophilic [^{99m}Tc/^{186}Re] Tc/Re-Tricarbonyl NODAGA and NOTA Complexes. *Nucl. Med. Biol.* **2019**, *71*, 39–46. DOI: 10.1016/j.nucmedbio.2019.04.004.

[15] (a) Booysen, I. N.; Ismail, M. B.; Akerman, M. P. Coordination Behavior of Chromone Schiff Bases Towards the $[Re^{V}O]^{3+}$ and $[Re^{I}(CO)_3]^{+}$ Cores. *J. Coord. Chem.* **2013**, 66, 4371–4386; (b) Booysen, I. N.; Ismail, M. B.; Munro, O. Q. Mono- and Dinuclear Rhenium(I) Compounds with Bidentate Benzimidazole Chelators. *Inorg. Chem. Commun.* **2013**, *30*, 168–172; (c) Booysen, I. N.; Ismail, M. B.; Gerber, T. I. A.; Akerman, M. P; van Brecht, B. Oxo and Oxofree Rhenium(V) Complexes with N,O-Donor Schiff Bases. *S.A. J. Chem.* **2012**, *65*, 174–177.

[16] (a) Johnson, N. P.; Lock, C. J. L.; Wilkinson, G. Complexes of Rhenium(V). *Inorg. Synth.* **1967**, *145*, 9; (b) Ciani, G.; Alfonso, G. D.; Romiti, P.; Sironi, A.; Freni, M. Rhenium(V) Oxide Complexes. Crystal and Molecular Structures of the Compounds Trans-$ReI_2O(OR)(PPh_3)_2$ (R = Et, Me) and of Their Hydrolysis Derivative $ReIO_2(PPh_3)_2$. *Inorg. Chim. Acta* **1983**, *72*, 29–37. DOI: 10.1016/S0020-1693(00)81690-4.

[17] *Bruker APEX2, SAINT and SADABS*. Bruker AXS Inc., **2010**., Madison, Wisconsin, USA. (software)

[18] Blessing, R. H. An Empirical Correction for Absorption Anisotropy. *Acta Crystallogr. A Found. Crystallogr.* **1995**, *A51*, 33–38. DOI: 10.1107/S0108767394005726.

[19] Sheldrick, G. M. A Short History of SHELX. *Acta Crystallogr. A Found. Crystallogr* **2008**, *64*, 112–122. DOI: 10.1107/S0108767307043930.

[20] Farrugia, L. J. J. WinGX and ORTEP for Windows: An Update. *J. Appl. Crystallogr.* **2012**, *45*, 849–854. DOI: 10.1107/S0021889812029111.

[21] Reichmann, M. F.; Rice, S. A.; Thomas, C. A.; Doty, P. A Further Examination of the Molecular Weight and Size of Desoxypentose Nucleic Acid. *J. Am. Chem. Soc.* **1954**, *76*, 3047–3053. DOI: 10.1021/ja01640a067.

[22] Kaplanis, M.; Stamatakis, G.; Papakonstantinou, V. D.; Paravatou-Petsotas, M.; Demopoulos, C. A.; Mitsopoulou, C. A. Re(I) Tricarbonyl Complex of 1,10-Phenanthroline-5,6-Dione: DNA Binding, Cytotoxicity, anti-Inflammatory and anti-Coagulant Effects Towards Platelet Activating Factor. *J. Inorg. Biochem.* **2014**, *135*, 1–9. DOI: 10.1016/j.jinorgbio.2014.02.003.

[23] Frisch, M. J.; Trucks, G. W.; Schlegel, H. B.; Scuseria, G. E.; Robb, M. A.; Cheeseman, J. R.; Scalmani, G.; Barone, V.; Mennucci, B.; Petersson, G. A.; et al. *Gaussian 09 (Revision A.01)*. Gaussian Inc.: Wallingford, CT, **2009**.

[24] Machura, B.; Kruszynski, R. Oxorhenium(V) complexes with Quinoline-2-Carboxylate Ligand. X-Ray Structure of $[ReOCl_2(Quin\text{-}2\text{-}c)(PPh_3)]$ and $[ReOBr_2(Quin\text{-}2\text{-}c)(AsPh_3)]$ Complexes: DFT and TD-DFT Calculations for [ReOCl2(Quin-2-c)(PPh_3)]. *Polyhedron* **2007**, *26*, 3686–3694. DOI: 10.1016/j.poly.2007.03.058.

[25] Brink, A.; Visser, H.; Roodt, A. Novel Imino Rhenium(I) tricarbonyl Complexes of Salicylidene-Derived Ligands: Synthesis, X-Ray Crystallographic Studies, Spectroscopic Characterization and DFT Calculations. *Polyhedron* **2013**, *52*, 416–423. DOI: 10.1016/j.poly.2012.08.059.

[26] Potgieter, K. C.; Gerber, T. I. A.; Betz, R.; Rhyman, L.; Ramasami, P. Structural and DFT/TD-DFT Investigation of Tris(Bidentate) Complexes of Rhenium(III) Synthesized from the *Cis*-$[ReO_2]^+$ Core and Benzenethiol Derivatives. *Polyhedron* **2013**, *59*, 91–100. DOI: 10.1016/j.poly.2013.04.038.

[27] Duhovny, D.; Nussinov, R.; Wolfson, H.J. International Workshop on Algorithms in Bioinformatics (WABI 2002): Algorithms in Bioinformatics, **2002**, 185–200. Schneidman-Duhovny, D.; Inbar, Y.; Nussinov, R.; Wolfson, H.J. PatchDock and SymmDock: Servers for Rigid and Symmetric Docking. *Nucl. Acids. Res.* **2005**, *33*, W363–W367. DOI: 10.1093/nar/gki481.

[28] Krieger, E.; Vriend, G. You Have Full Text Access to This OnlineOpen Article New Ways to Boost Molecular Dynamics Simulations. *J. Comput. Chem.* **2015**, *36*, 996–1007. DOI: 10.1002/jcc.23899.

[29] Kang, Y.; Ito, A.; Sakuda, E.; Kitamura, N. Diimine Ligand Structure Effects on Photophysical Properties of Tricarbonyl Rhenium(I) complexes Having Arylborane Charge Transfer Units. *J. Photochem. Photobiol. A* **2015**, *313*, 107–116. DOI: 10.1016/j.jphotochem.2015.05.034.

[30] Banerjee, S. R.; Levadala, M. K.; Lazarova, N.; Wei, L.; Valliant, J. F.; Stephenson, K. A.; Babich, J. W.; Maresca, K. P. Zubieta, Bifunctional Single Amino Acid Chelates for Labeling of Biomolecules with the $\{Tc(CO)_3\}^+$and $\{Re(CO)_3\}^+$ Cores. Crystal and Molecular Structures of $[ReBr(CO)_3(H_2NCH_2C_5H_4N)]$, $[Re(CO)_3\{(C_5H_4NCH_2)_2NH\}]Br$, $[Re(CO)_3\{(C_5H_4NCH_2)_2NCH_2CO_2H\}]Br$, $[Re(CO)_3\{X(Y)NCH_2CO_2CH_2CH_3\}]Br$ (X = Y = 2-Pyridylmethyl; X = 2-Pyridylmethyl, Y = 2-(1-Methylimidazolyl)Methyl; X = Y = 2-(1-Methylimidazolyl)Methyl), $[ReBr(CO)_3\{(C_5H_4NCH_2)NH(CH_2C_4H_3S)\}]$, and $[Re(CO)_3\{(C_5H_4NCH_2)N(CH_2C_4H_3S)(CH_2CO_2)\}]$. *J. Inorg. Chem.* **2002**, *41*, 6417–6425. DOI: 10.1021/ic020476e.

[31] Mayer, P.; Gerber, T. I. A.; Buyambo, B.; Abrahams, A. Coordination Behaviour of Acetylacetone-Derived Schiff Bases Towards Rhenium(I) and (V). *Polyhedron* **2009**, *28*, 1174–1178. DOI: 10.1016/j.poly.2009.01.036.

[32] Zhang, H.; Yang, F.; Wu, Q.; Liao, S.-Y.; Liu, P.; Mei, W.-J.; Li, L.; Zhang, S.-Y.; Wang, X.-C. Synthesis, DNA-Binding Properties and Quantitative Structure-Activity Relationships on Ruthenium(II) Complexes with Calf-Thymus DNA. *Med. Chem. (Los Angeles)* **2016**, *6*, 137–142.

[33] Zianna, A.; Psomas, G.; Hatzidimitriou, A.; Lalia-Kantouri, M. Copper(II) Complexes of Salicylaldehydes and 2-Hydroxyphenones: synthesis, Structure, Thermal Decomposition Study and Interaction with Calf-Thymus DNA and Albumins. *RSC Adv.* **2015**, *5*, 37495–37511. DOI: 10.1039/C4RA16484A.

[34] Barone, G.; Gambino, N.; Ruggirello, A.; Silvestri, A.; Terenzi, A.; Liveri, V. T. Spectroscopic Study of the Interaction of Ni^{II}-5-Triethyl Ammonium Methyl Salicylidene Ortho-Phenylendiiminate with Native DNA. *J. Inorg. Biochem.* **2009**, *103*, 731–737. DOI: 10.1016/j.jinorgbio.2009.01.006.

[35] Silvestri, A.; Barone, G.; Ruisi, G.; Anselmo, D.; Riela, S.; Liveri, V. T. The Interaction of Native DNA with Zn(II) and Cu(II) Complexes of 5-Triethyl Ammonium Methyl Salicylidene Orto-Phenylendiimine. *J. Inorg. Biochem.* **2007**, *101*, 841–848. DOI: 10.1016/j.jinorgbio.2007.01.017.

[36] Khan, N. H.; Pandya, N.; Prathap, K. J.; Kureshy, R. I.; Abdi, S. H. R.; Mishra, S.; Bajaj, H. C. The Interaction of Native DNA with Zn(II) and Cu(II) Complexes of 5-Triethyl Ammonium Methyl Salicylidene Orto-Phenylendiimine. *Spectrochim. Acta A* **2011**, *81*, 199–208.

[37] Kurdekar, G. S.; Puttanagouda, S. M.; Kulkarni, N. V.; Budagumpi, S.; Revankar, V. K. Synthesis, Characterization, Antibiogram and DNA Binding Studies of Novel Co(II), Ni(II), Cu(II), and Zn(II) Complexes of Schiff Base Ligands with Quinoline Core. *Med. Chem. Res.* **2011**, *20*, 421–429. DOI: 10.1007/s00044-010-9330-5.

[38] Chaudhary, K. K.; Mishra, N. A Review on Molecular Docking: Novel Tool for Drug Discovery. *JSM Chem.* **2016**, *4*, 1029.

[39] Thamilarasan, V.; Jayamani, A.; Sengottuvelan, N. Synthesis, Molecular Structure, Biological Properties and Molecular Docking Studies on Mn^{II}, Co^{II} and Zn^{II} Complexes Containing Bipyridine–Azide Ligands. *Eur. J. Med. Chem.* **2015**, *89*, 266–278. DOI: 10.1016/j.ejmech.2014.09.073.

[40] Kyros, L.; Banti, C. N.; Kourkoumelis, N.; Kubicki, M.; Sainis, I.; Hadjikakou, S. K. Synthesis, Characterization, and Binding Properties Towards CT-DNA and Lipoxygenase of Mixed-Ligand Silver(I) complexes with 2-Mercaptothiazole and Its Derivatives and Triphenylphosphine. *J. Biol. Inorg. Chem.* **2014**, *19*, 449–464. DOI: 10.1007/s00775-014-1089-6.

[41] Quiroga, E. D.; Cormick, M. P.; Pons, P.; Alvarez, M. G.; Durantini, E. N. Mechanistic Aspects of the Photodynamic Inactivation of Candida albicans Induced by Cationic Porphyrin Derivatives. *Eur. J. Med. Chem.* **2012**, *58*, 332–339. DOI: 10.1016/j.ejmech.2012.10.018.

[42] Pratviel, G.; Bernadou, J.; Meunier, B. DNA and RNA Cleavage by Metal Complexes. *Adv. Inorg. Chem.* **1998**, *45*, 251–312.

[43] Xu, Z.-H.; Chen, F.-J.; Xi, P.-X.; Liu, X.-H.; Zeng, Z.-Z. Synthesis, Characterization, and DNA-Binding Properties of the Cobalt(II) and Nickel(II) Complexes with Salicylaldehyde 2-Phenylquinoline-4-Carboylhydrazone. *J. Photochem. Photobiol. A* **2008**, *196*, 77–83. DOI: 10.1016/j.jphotochem.2007.11.017.

[44] Barton, J. K.; Danishefsky, A. T.; Goldberg, J. M. Tris(Phenanthroline)Ruthenium(II): Stereoselectivity in Binding to DNA. *J. Am. Chem. Soc.* **1984**, *106*, 2172–2176. DOI: 10.1021/ja00319a043.

[45] Chow, C. S.; Barton, J. K. Transition Metal Complexes as Probes of Nucleic Acids. *Methods Enzymol.* **1992**, *212*, 219–242.

[46] Shakir, M.; Abbasi, A.; Khan, A. U.; Khan, S. N. Synthesis and Spectroscopic Studies on the Schiff Base Ligand Derived from Condensation of 2-furaldehyde and 3,3'-diaminobenzidene, L and its complexes with Co(II), Ni(II), Cu(II) and Zn(II): comparative DNA binding studies of L and its Cu(II) and Zn(II) complexes. *Spectrochim. Acta. A Mol. Biomol. Spectrosc.* **2011**, *78*, 29–35. DOI: 10.1016/j.saa.2010.02.034.

[47] Arjmand, F.; Sayeed, F.; Muddassir, M. Synthesis of New Chiral Heterocyclic Schiff Base Modulated Cu(II)/Zn(II) Complexes: Their Comparative Binding Studies with CT-DNA, Mononucleotides and Cleavage Activity. *J. Photochem. Photobiol. B* **2011**, *103*, 166–179. DOI: 10.1016/j.jphotobiol.2011.03.001.

[48] Shi, J.-H.; Chen, J.; Wang, J.; Zhu, Y.-Y. Binding Interaction between Sorafenib and Calf Thymus DNA: Spectroscopic Methodology, Viscosity Measurement and Molecular Docking. *Spectrochim. Acta Part A* **2015**, *136*, 443–450. DOI: 10.1016/j.saa.2014.09.056.

[49] Shi, J.-H.; Liu, T.-T.; Jiang, M.; Chen, J.; Wang, Q. Characterization of Interaction of Calf Thymus DNA with Gefitinib: Spectroscopic Methods and Molecular Docking. *J. Photochem. Photobiol. B* **2015**, *147*, 47–55. DOI: 10.1016/j.jphotobiol.2015.03.005.

[50] Alonso, H.; Bliznyuk, A. A.; Gready, J. E. Combining Docking and Molecular Dynamic Simulations in Drug Design. *Med. Res. Rev.* **2006**, *26*, 531–568. DOI: 10.1002/med.20067.

[51] Shahabadi, N.; Darabi, F.; Maghsudi, M.; Kashanian, S. DNA Binding and Gel Electrophoresis Studies of a Copper (II) Complex Containing Mixed Aliphatic and Aromatic Dinitrogen Ligands, *DNA. Cell Biol.* **2010**, *29*, 329–336. DOI: 10.1089/dna.2009.1001.

[52] Chen, J.; Huang, Y.-W.; Liu, G.; Afrasiabi, Z.; Sinn, E.; Padhye, S.; Ma, Y. The Cytotoxicity and Mechanisms of 1,2-Naphthoquinone Thiosemicarbazone and Its Metal Derivatives against MCF-7 Human Breast Cancer Cells. *Toxicol. Appl. Pharmacol.* **2004**, *197*, 40–48. DOI: 10.1016/j.taap.2004.02.004.

[53] Abdel-Rahman, L. H.; El-Khatib, R. M.; Nassr, L. A. E.; Abu-Dief, A. M.; Ismael, M.; Seleem, A. A. Metal Based Pharmacologically Active Agents: Synthesis, Structural Characterization, Molecular Modeling, CT-DNA Binding Studies and in Vitro Antimicrobial Screening of Iron(II) Bromosalicylidene Amino Acid Chelates. *Spectrochim. Acta A* **2014**, *117*, 366–378. DOI: 10.1016/j.saa.2013.07.056.

[54] Kashanian, S.; Shariati, Z.; Roshanfekr, H.; Ghobadi, S. DNA Binding Studies of 3,5,6-Trichloro-2-Pyridinol Pesticide Metabolite. *DNA Cell Biol.* **2012**, *31*, 1341–1348. DOI: 10.1089/dna.2012.1662.